JOURNAL OF MATERIALS SCIENCE 24 (1989) 76–82

Morphology and formation mechanism of the pyrochlore phase in ZnO varistor materials

JONG CHOUL KIM, EDWARD GOO
Department of Materials Science and Engineering, University of Southern California, Los Angeles, California 90089-0241, USA

The secondary phases in ZnO varistor materials, having Bi_2O_3, Sb_2O_3, $MnCO_3$ and CoO as additives, were investigated using transmission electron microscopy with an energy dispersive X-ray spectrometer and X-ray diffractometer scans. The information about the morphology of the pyrochlore phase and its formation reaction were obtained. The pyrochlore phase is formed from the reaction between the spinel and Bi_2O_3 phase. Below 1200° C, the spinel phase reacts with the liquid Bi_2O_3 phase present at the multiple grain junction and forms the pyrochlore phase. The pyrochlore phase nucleates at the corners of multiple grain junction adjacent to the spinel grain and grows towards the centre of the grain junction.

1. Introduction

Because of the highly nonlinear current–voltage characteristics of ZnO varistors [1], they are used as protection devices against voltage surges. The major applications are in the protection of solid state devices and electric power generation systems [2].

The desired property of a varistor is that it be a perfect insulator up to the breakdown voltage and becomes highly conductive above the breakdown voltage. The current–voltage characteristics of varistor above the breakdown voltage can be expressed by the equation $I = (V/C)\alpha$ [1], where I and V are the current and voltage and α and C are constants. Therefore, a higher alpha is desired because it means a larger change in current for a given voltage change above the breakdown voltage.

It was found that certain oxide additions substantially increase the value of α in ZnO varistors. Much of the information on the effect of oxide additions on the value of alpha was initially reported by Matsuoka [1]. Alpha values around 50 are obtained by the additions of Bi_2O_3, Sb_2O_3 and the transition metal oxides such as MnO, CoO and Cr_2O_3.

The oxide additions result in the formation of secondary phases. Although the secondary phases have no direct effects on the non-ohmic properties, they may affect the macroscopic electrical properties through their effects on the microstructure development during sintering and grain growth. In order to understand their effects completely, information about the morphology of secondary phases and their formation reactions is essential.

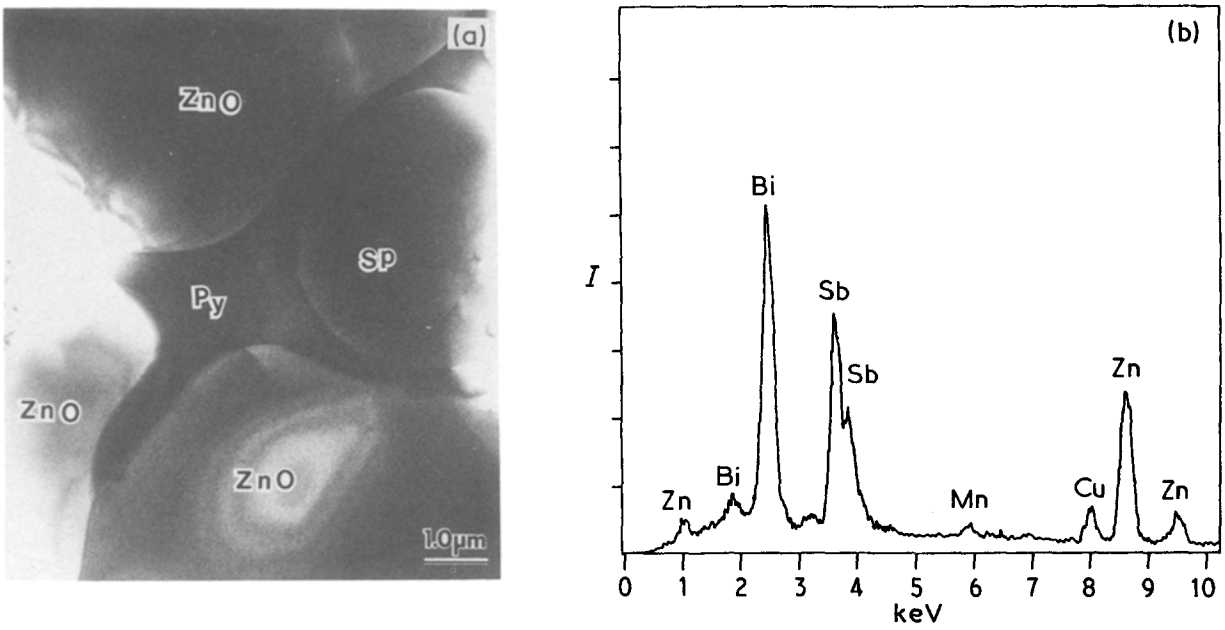

Figure 1 (a) Bright-field image of the pyrochlore phase, which is present as an intergranular phase, taken from the sample sintered at 1200° C. Py: pyrochlore phase, Sp: spinel phase. (b) EDS spectrum taken from the pyrochlore phase.

0022–2461/89 $03.00 + .12

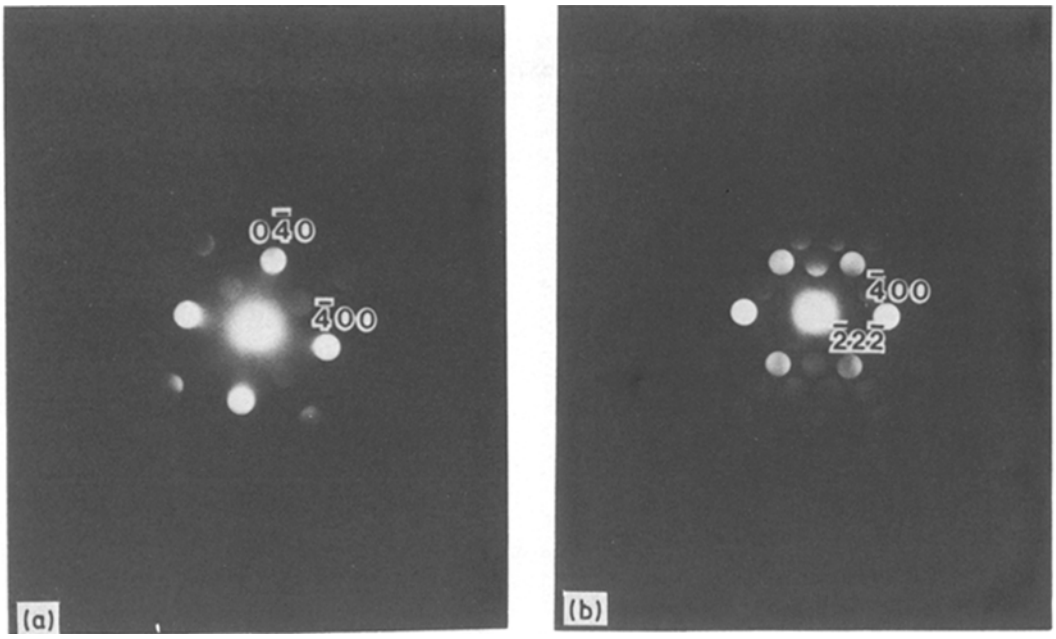

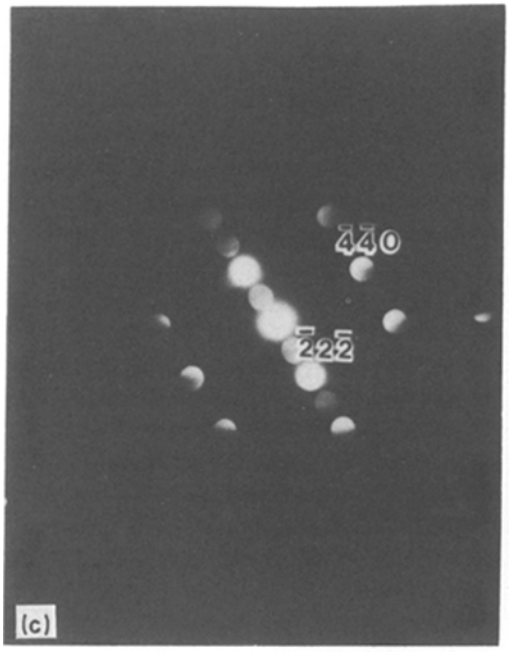

Figure 2 Electron microdiffraction patterns from the pyrochlore phase shown in Fig. 1. (a) [0 0 1] zone axis, (b) [0 1 1] zone axis, (c) [$\bar{1}$ 1 2] zone axis.

Most of the microstructural characterization has been done on the ZnO varistors which were processed under optimal conditions to produce the maximum alpha value. Typical microstructure of ZnO varistor materials consists of ZnO grains with a grain size in the range 10 to 20 μm. Among the ZnO grains, the spinel phase is present as grains 1 to 2 μm diameter.

It was believed that a continuous intergranular bismuth oxide phase, which isolates the ZnO grains completely, was responsible for the non-ohmic behaviour [3–5]. However, later investigations [6–8] using direct observation in the transmission electron microscope have shown that the bismuth oxide phase is present primarily at multiple grain junctions and is not a continuous grain-boundary phase. At room temperature the bismuth oxide phase is crystalline;

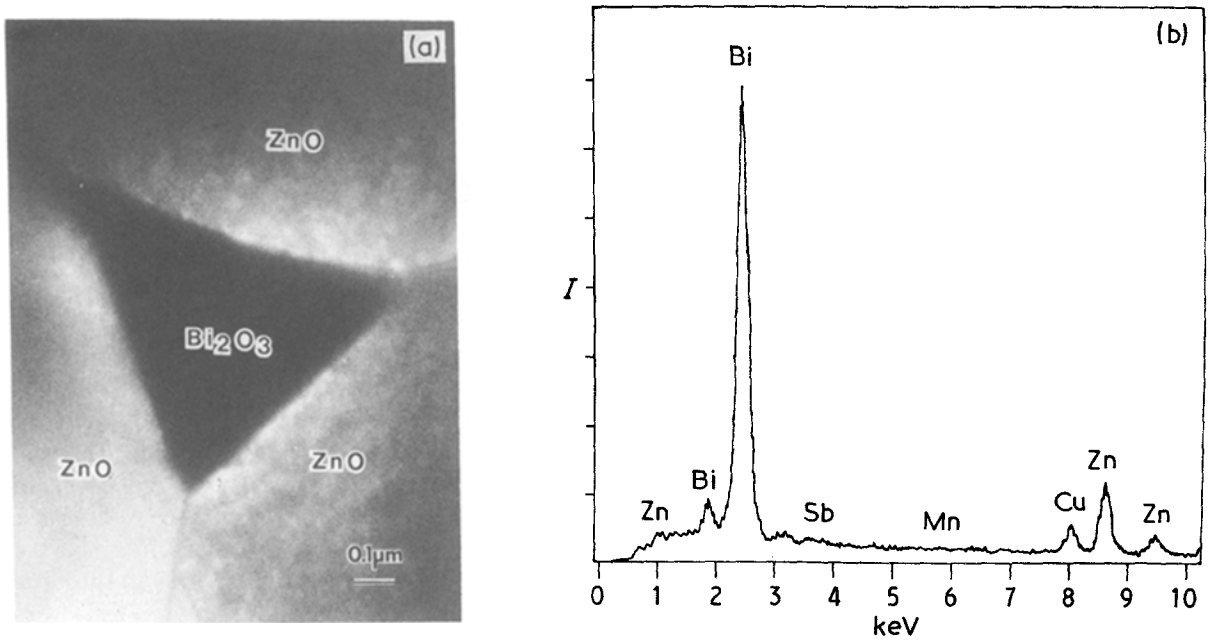

Figure 3 (a) Bright-field image of the Bi_2O_3 phase located at the multiple grain junction taken from the sample sintered at 1200° C. (b) EDS spectrum taken from the Bi_2O_3 phase.

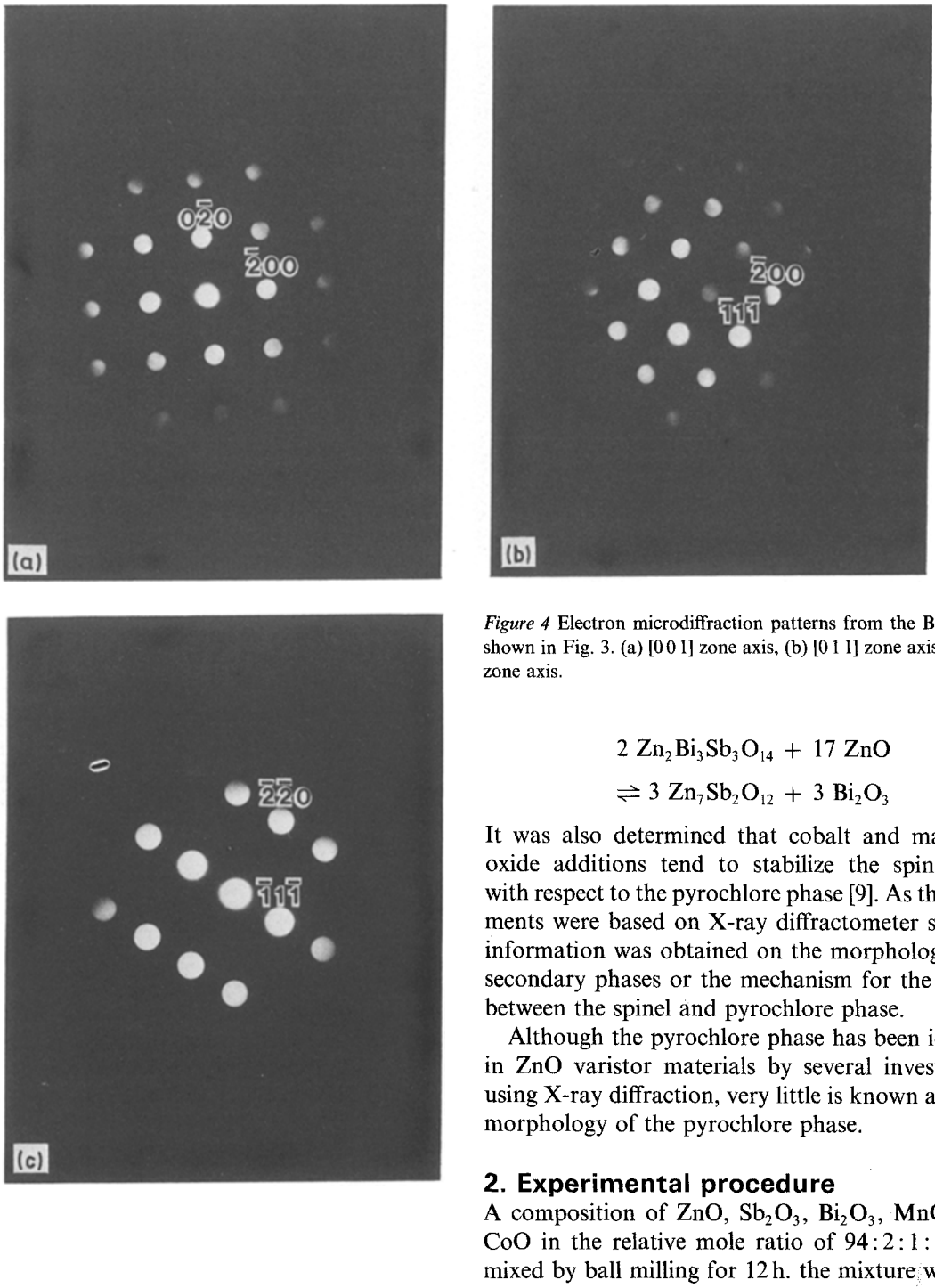

Figure 4 Electron microdiffraction patterns from the Bi_2O_3 phase shown in Fig. 3. (a) [0 0 1] zone axis, (b) [0 1 1] zone axis, (c) [$\bar{1}$ 1 2] zone axis.

however, it may exist in several crystalline forms depending on cooling rates and the presence of transition metal oxide additions [9].

An extensive investigation of the formation of the secondary phases and the reactions between the various phases in ZnO was undertaken by Inada [9, 10]. X-ray diffractometer scans were used to determine the phases present as a function of sintering temperature, cooling rate and amount of transition metal oxides added.

The composition of spinel phase was postulated to be $Zn_7Sb_2O_{12}$ with lattice parameter $a = 0.85$ nm [9, 11]. He found that the pyrochlore phase, which was postulated to have the composition $Zn_2Bi_3Sb_3O_{14}$ with a lattice constant 1.040 nm, was stable at low temperatures (700 to 900° C), and at higher temperatures it transforms to the spinel and bismuth oxide phases as shown in Equation 1 [9].

$$2\ Zn_2Bi_3Sb_3O_{14} + 17\ ZnO \rightleftharpoons 3\ Zn_7Sb_2O_{12} + 3\ Bi_2O_3 \quad (1)$$

It was also determined that cobalt and manganese oxide additions tend to stabilize the spinel phase with respect to the pyrochlore phase [9]. As the experiments were based on X-ray diffractometer scans, no information was obtained on the morphology of the secondary phases or the mechanism for the reaction between the spinel and pyrochlore phase.

Although the pyrochlore phase has been identified in ZnO varistor materials by several investigations using X-ray diffraction, very little is known about the morphology of the pyrochlore phase.

2. Experimental procedure

A composition of ZnO, Sb_2O_3, Bi_2O_3, $MnCO_3$ and CoO in the relative mole ratio of 94:2:1:1:1 was mixed by ball milling for 12 h. the mixture was dried and cold pressed into discs of 1 in. (~2.54 cm) diameter. Pressed samples were sintered at 1200 and 1300° C followed by air cooling. The samples sintered at 1300° C were annealed at 1100 and 900° C for 1 h.

Specimens for transmission electron microscopy (TEM) were prepared by cutting 3 mm diameter discs using a ultrasonic cutter and followed by thinning down to less than 100 μm by mechanical grinding with SiC paper and polishing with Al_2O_3 powder. The specimens were then thinned in a Gatan model 600 dual ion-milling machine with argon ions with a 6 kV acceleration voltage. The examination of the morphology of the secondary phases was carried out on a Philips 420 transmission electron microscope (TEM) with an energy dispersive X-ray spectrometer (EDS).

The 1300° C sintered sample and two annealed samples were ground into powder for X-ray analysis.

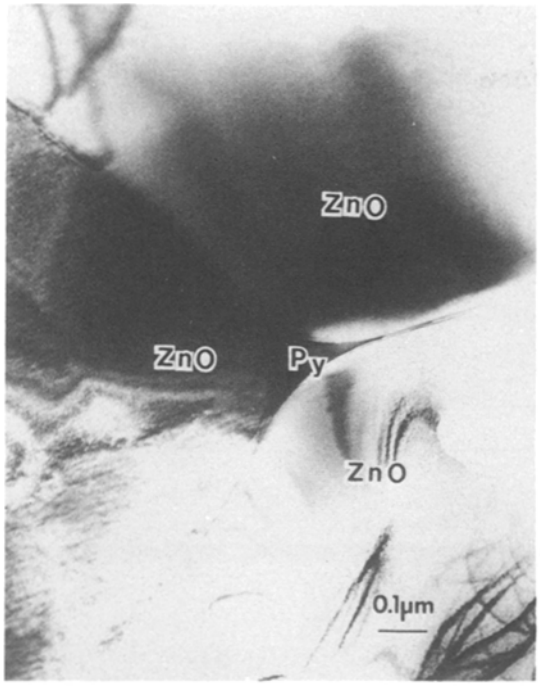

Figure 5 Bright-field image of the pyrochlore phase (Py) located at the multiple grain junction in the sample sintered at 1300° C.

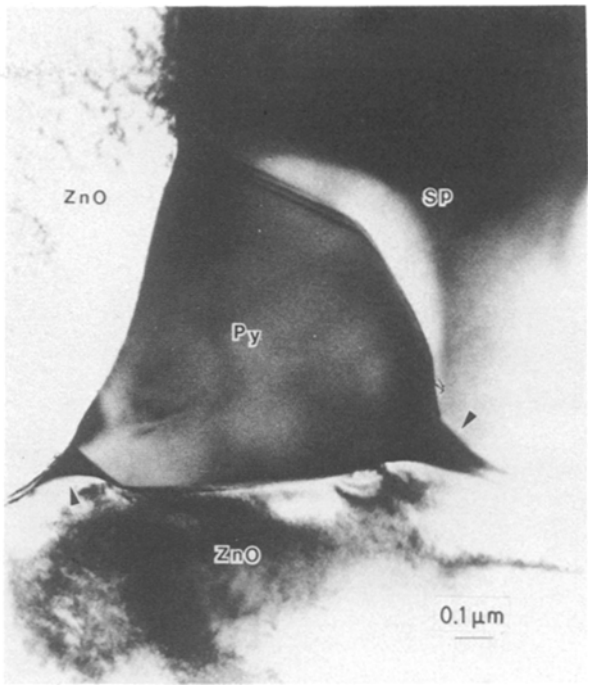

Figure 6 Bright-field image of the pyrochlore phase (Py) located at the multiple grain junction with Bi_2O_3 phase (arrows) in the sample annealed at 900° C for 1 h. Sp: spinel phase.

X-ray diffractometer scan was done at 1° min^{-1} scanning rate using Gu$K\alpha$ X-rays.

3. Results

For the samples sintered at 1200° C, we found the pyrochlore phase present as an intergranular phase with a thickness of 0.5 to 1.0 μm. Fig. 1a shows a bright-field image, from the sample sintered at 1200° C, of the pyrochlore phase. The EDS spectrum shown in Fig. 1b, taken from the intergranular phase, shows it contains zinc, bismuth and antimony. In addition, the microdiffraction patterns from the same phase are shown in Fig. 2. These results confirm that the intergranular phase is the pyrochlore phase. The pyrochlore phase is always found at a multiple grain junction and is often adjacent to a spinel grain. Spinel phase is surrounded by the pyrochlore phase in Figure 1a. Nearly all the pyrochlore phase in the 1200° C sintered sample has this morphology.

Fig. 3a shows the bright-field image from the sample sintered at 1200° C of Bi_2O_3 which is located at the multiple grain junctions and surrounded by ZnO grains. Figs 3b and 4 are the EDS spectrum and microdiffraction patterns taken from the same area. This phase was identified as δ-Bi_2O_3 phase having a cubic structure.

Samples sintered at 1300° C had only small amounts of the pyrochlore phase. In addition, the pyrochlore phase is present at the multiple grain junction surrounded by ZnO grains and terminates with a small dihedral angle as shown in Fig. 5.

Annealing the sample sintered at 1300° C for 1 h at 1100° C resulted in the formation of the pyrochlore phase. Fig. 6 is the bright-field image of the pyrochlore phase which is present at the multiple grain junction. The spinel phase is located at the upper right. A common feature of the morphology of the pyrochlore

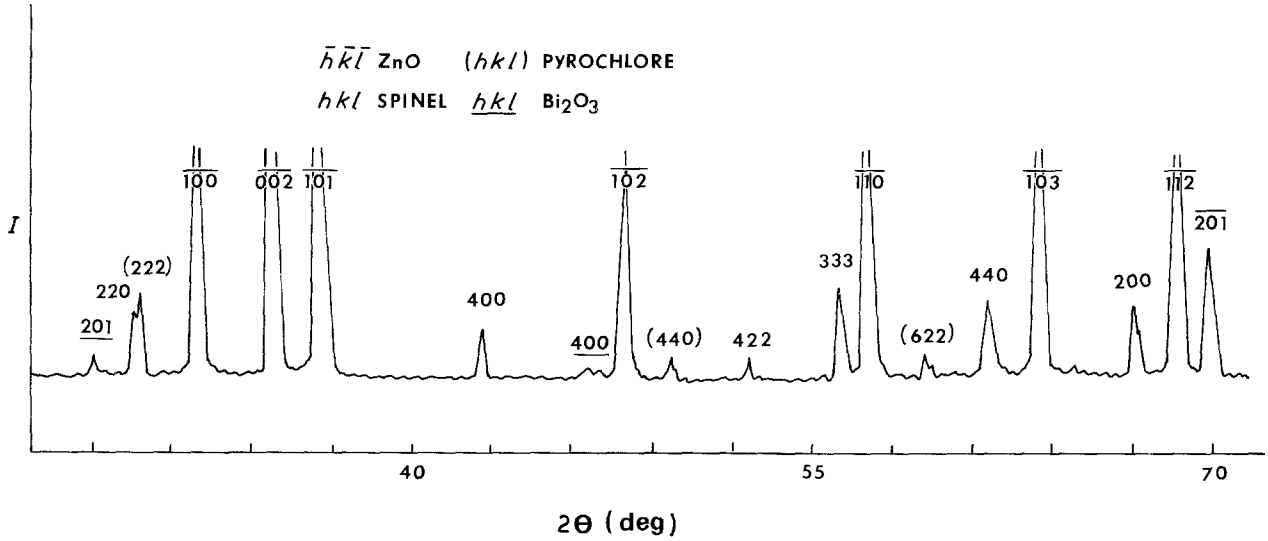

Figure 7 The indexed X-ray diffractometer scan from the 900° C annealed sample.

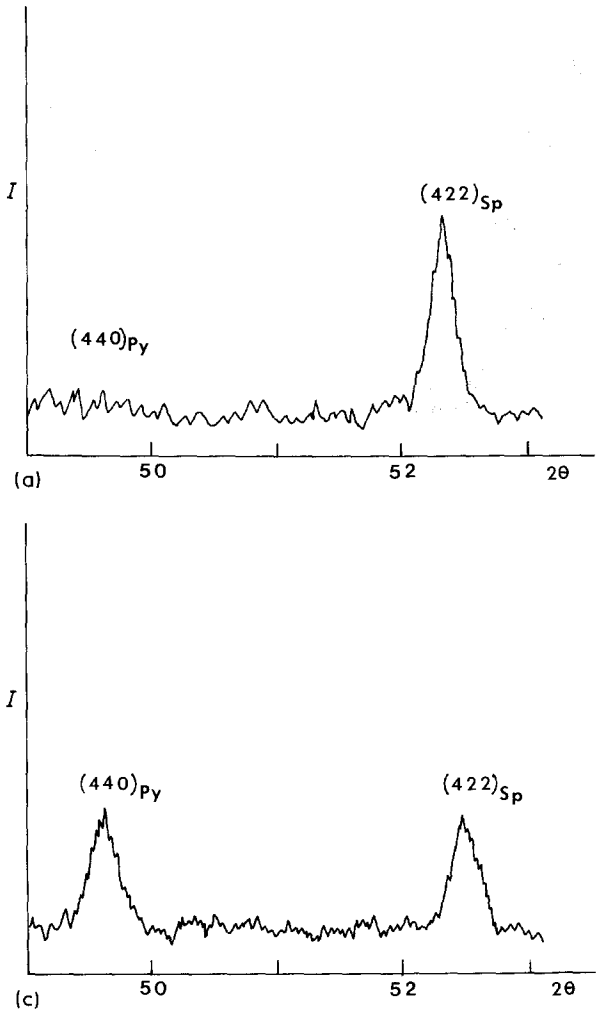

Figure 8 The intensity change of the (4 2 2) spinel and (4 4 0) pyrochlore phase peaks with annealing. (a) As-sintered sample at 1300° C, (b) annealed at 1100° C, (c) annealed at 900° C.

phase in annealed samples is that the interface between pyrochlore and spinel phase bulges towards the spinel grain as seen in Fig. 6. The Bi_2O_3 phase is also located at the multiple grain junctions adjacent to the ZnO grains and separated from the spinel grain by the pyrochlore phase. The Bi_2O_3 phase is generally surrounded by ZnO grains. There is no significant difference in microstructure for the samples annealed at 900 and 1100° C except for a slight increase in the amount of pyrochlore phase for the sample annealed at 900° C.

Fig. 7 shows the indexed X-ray intensity peaks taken from 900° C annealed sample. Fig. 8 shows the intensity change of the (4 2 2) spinel and (4 4 0) pyrochlore phase peaks with annealing. The X-ray intensity data are summarized in Fig. 9. X-ray peaks were normalized with respect to the intensity of (2 0 0) ZnO peaks. The data show that annealing increases the amounts of pyrochlore phase and decreases the amount of spinel phase. The lattice constant of the pyrochlore phase was calculated at 1.036 nm and that of spinel as 0.852 nm.

4. Discussion

Our X-ray results indicate that the volume fraction of pyrochlore phase increases upon annealing while the volume fraction of spinel phase and Bi_2O_3 phase decreases. This supports the phase transformation reaction proposed by Inada [9]. However, Inada reported that the pyrochlore phase is stable at temperatures below 900° C. Our results show that the temperature below which the pyrochlore phase is stable lies between 1200 and 1300° C.

In addition to the X-ray results, TEM with EDS results provide microstructural evidence that the phase transformation reaction is correct. The pyrochlore phase is often found adjacent to the spinel phase. This morphology strongly suggests that the spinel phase reacts to transform to the pyrochlore phase.

In addition, nearly all of the multiple grain junctions were occupied by the Bi_2O_3 phase before annealing. However, after annealing, the pyrochlore phase is found at the multiple grain junctions bordered by at least one spinel grain. The interface between spinel and pyrochlore phase is found to bulge toward the spinel phase as shown in Fig. 6.

Based on this information, the following mechanism for the transformation is proposed. The Bi_2O_3 phase is present as a liquid at the multiple grain junction at the annealing temperature which is above its melting temperature of 825° C [12]. For the transformation to occur, it is surrounded by ZnO grains and at least one spinel grain. The pyrochlore phase becomes more stable than the spinel phase, and nucleation of the pyrochlore phase starts at the corners of the multiple grain junction from the reaction between the spinel and Bi_2O_3 phase. The spinel phase dissolves into the Bi_2O_3 phase and growth occurs at the pyrochlore/Bi_2O_3 interface. The pyrochlore nucleus grows towards the centre of the multiple grain junction.

From the thermodynamical point of view, the corners of the multiple grain junction are the most probable nucleation sites because they have a smaller activation energy barrier for the nucleation due to the small volume of nuclei for the critical radius (r^*) of the nucleation. The nucleation starts at the corners adjacent to the spinel phase. Once the pyrochlore phase covers the spinel phase, the dissolution of the spinel phase into the Bi_2O_3 liquid will effectively be stopped. Therefore, the spinel phase furthest from the corners will be dissolved into the Bi_2O_3 phase to a

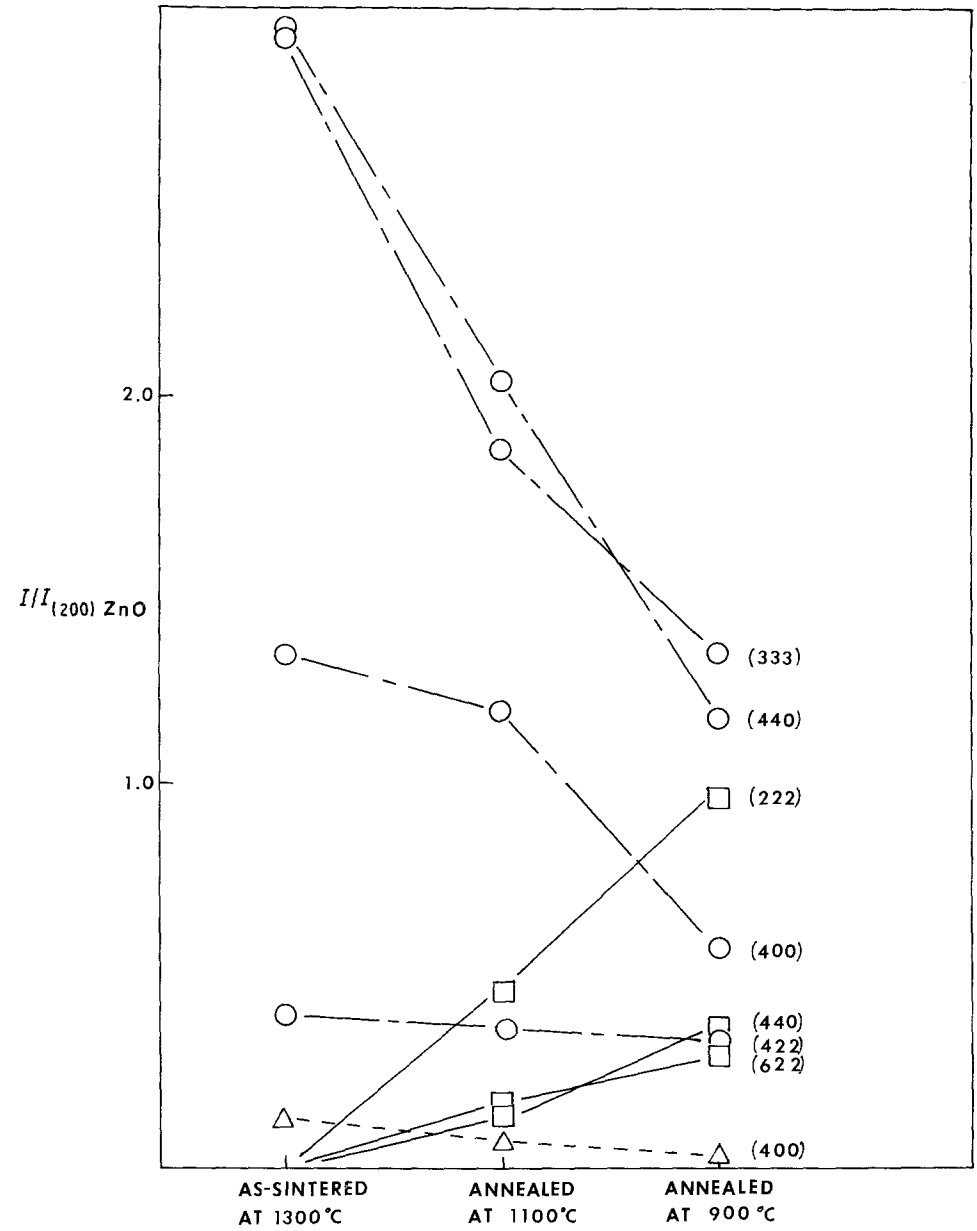

Figure 9 Summary of the X-ray results. (○) Spinel, (□) pyrochlore, (△) Bi_2O_3.

greater extent. This results in the interface of spinel/pyrochlore phase bulging towards the spinel phase.

The resulting ZnO phase from the reaction may be deposited adjacent to the ZnO grains through diffusion in liquid Bi_2O_3 phase. This causes a slight growth of the ZnO grains adjacent to the multiple grain junction, but the ZnO grain morphology will not be changed. A schematic illustration of the formation mechanism for the pyrochlore phase is shown in Fig. 10.

Because the pyrochlore phase has been grown from the corners, it may have more than two crystallographic orientations. In Fig. 11, the grain junction is surrounded by only ZnO grains and two pyrochlore phases exist at the same grain junction. The micrograph is a section through the multiple grain junction, and therefore it is possible for the spinel grain to be above or below the multiple grain junction shown in Fig. 11.

In the 1200° C sintered sample, the pyrochlore phase is present as an intergranular phase with a thickness of 0.5 to 1.0 μm as shown in Fig. 1a. Because the sintering and formation of the pyrochlore phase occurred simultaneously for the sample sintered at 1200° C, it is expected that the pyrochlore morphology would differ from the annealed samples. Determining the mechanism of the pyrochlore phase formation during sintering is difficult.

In the 1300° C sintered sample, the small amount of pyrochlore phase that is present is mainly located at the multiple grain junction. This morphology change can be explained by assuming the melting temperature of pyrochlore phase is between 1200 and 1300° C. Inada [4] has reported the melting point of pyrochlore to be 1280° C.

5. Conclusions

Our investigation shows that the pyrochlore phase is formed from the reaction between spinel and Bi_2O_3 phase. The pyrochlore phase is stable at temperatures below 1200° C and spinel phase reacts with the Bi_2O_3 phase which is present at the multiple grain junction to form the pyrochlore phase. The nucleation of the pyrochlore phase starts at the corners of the multiple

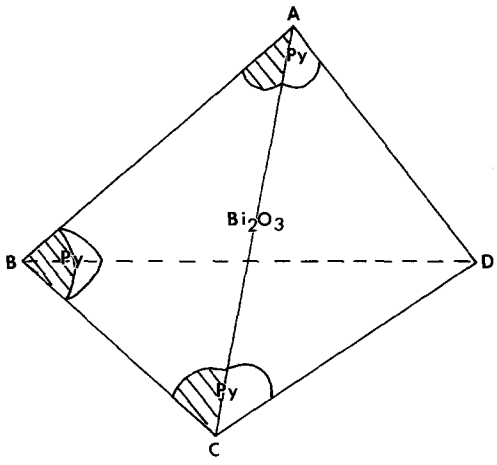

(a)

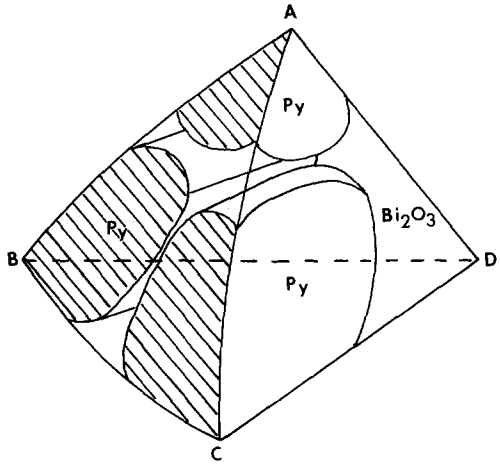

(b)

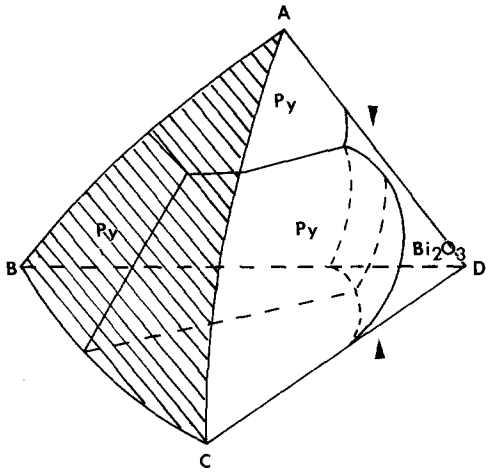

(c)

Figure 10 Schematic drawings for the phase transformation mechanism. (a) Nucleation, (b) growth, (c) final morphology.

grain junction adjacent to the spinel grain and grows towards the centre of the multiple grain junction with matter transport occurring through the liquid Bi_2O_3 phase.

The morphology of the pyrochlore phase is different for the sample sintered at 1200° C. For these samples, the pyrochlore phase is present as an intergranular phase adjacent to the spinel phase.

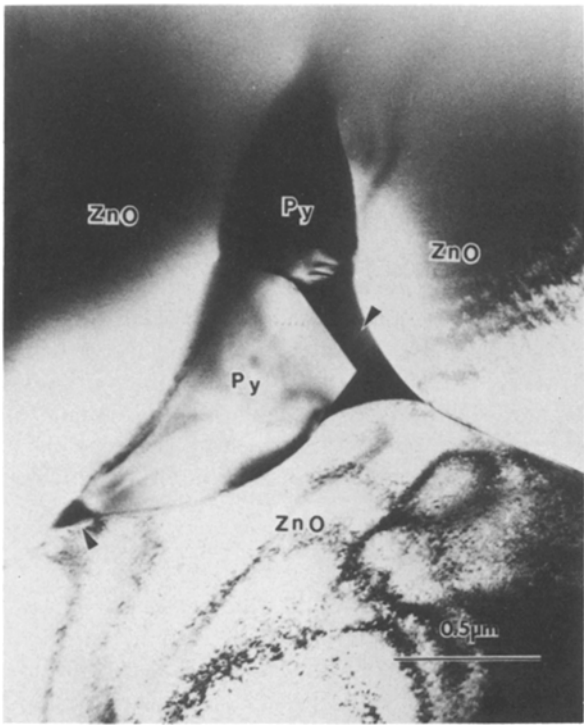

Figure 11 Bright-field image showing two pyrochlore grains (Py) at the multiple grain junction from the sample annealed at 900° C. Arrows point to the Bi_2O_3 phase.

Acknowledgements

The authors thank the Center for Electron Microscopy and Microanalysis (CEMMA) at USC for use of their facilities. We also thank Dr John Porter and Mr Joe Ratto at the Rockwell International Science Center for their help with X-ray diffractometer scans.

References

1. M. MATSUOKA, *Jpn J. Appl. Phys.* **10** (1971) 736.
2. L. M. LEVINSON and H. R. PHILIPP, *IEEE Trans. Parts. Hybrid Packaging* **PAP-13** (1977) 338.
3. W. G. MORRIS, *J. Amer. Ceram. Soc.* **56** (1973) 360.
4. J. WONG, P. RAO and E. F. KOCH, *J. Appl. Phys.* **47** (1975) 1827.
5. M. INADA, *Jpn J. Appl. Phys.* **17** (1978) 173.
6. D. R. CLARKE, *J. Appl. Phys.* **49** (1978) 2407.
7. A. T. SANTHANAM, T. K. GUPTA and W. G. CARLSON, *ibid.* **50** (1979) 852.
8. H. KANAI, H. IMAI and T. TAKAHASHI, *J. Mater. Sci.* **24** (1985) 3957.
9. M. INADA, *Jpn J. Appl. Phys.* **19** (1980) 409.
10. *Idem, ibid.* **17** (1978) 1.
11. J. WONG, *ibid.* **46** (1975) 1653.
12. E. M. LEVIN, in "Phase diagrams for ceramists", 2nd Edn, The American Ceramic Society, Columbus, Ohio (1969).

Received 16 December 1987
and accepted 6 May 1988